Design of Passive Common-Mode Attenuation Methods for Inverter-Fed Induction Motor Drive With Reduced Common-Mode Voltage PWM Technique

Kalaiselvi Jayaraman and Manish Kumar, *Student Member, IEEE*

***Abstract*—This paper investigates the influence of active zero vector pulsewidth modulation (AZPWM-1) and space vector pulsewidth modulation (SVPWM) on the design of passive common-mode (CM) attenuation methods to reduce CM current and shaft voltage in inverter-fed V/f-controlled induction motor drives. The passive CM attenuation methods examined here are the CM choke, the CM electromagnetic interference (EMI) filter, and the CM transformer. The attenuation requirement of AZPWM-1 and SVPWM is identified to design the passive CM choke and EMI filter. Based on the attenuation requirement, the design guidelines are revisited for SVPWM, and design rules are proposed for AZPWM-1. However, the CM transformer is designed based on the step change in magnitude of CM voltage of both the pulsewidth modulations (PWMs). The limitations in design, regarding switching frequency and component size for each case, are also established. It is shown that to have a similar attenuation in the considered two PWM cases, AZPWM-1 requires smaller passive components compared to SVPWM. The proposed design guidelines are substantiated with experimental results on a 1.1-kW induction motor drive.**

***Index Terms*—Active zero vector pulsewidth modulation (AZPWM-1), common-mode choke, common-mode current (CMC), common-mode filter, common-mode transformer (CMT), induction motor (IM) drive, shaft voltage, size reduction, space vector pulsewidth modulation (SVPWM).**

I. Introduction

VARIABLE-FREQUENCY drives (VFDs), despite their enormous advantages, suffer certain setbacks. Common-mode (CM) issues are prevalent in VFDs, which are augmented by the faster switching capabilities of active devices. These CM components, in turn, cause distortions in the control signals and instigate disturbances in the surrounding systems [1]. Such CM components are the primary sources of shaft voltage, bearing current, and insulation failures in VFDs, which render the system unreliable and expensive [1]–[3]. The aforementioned CM issues in pulsewidth modulation (PWM)-fed inverter drives are addressed through control algorithms, PWM techniques, and active and passive methods.

An active method uses a precise combination of switches, inductors, capacitors, and appropriate control techniques primarily to reduce the size of hardware and to eliminate the common-mode voltage (CMV) in a wide frequency range [4]–[9]. For instance, a hybrid active filter [4], an active filter circuit with a common-mode transformer (CMT) [5], [9], and circuits based on current-controlled current-source techniques [6] have been proposed to nullify the CMV at machine terminals. The design of active methods is not only complex (attenuation and phase requirement needs precise tuning over the frequency range), but also strongly dependent on the rating of the drive. Also, active switches introduce additional power loss, increase the control complexity, and decrease reliability [6].

As the name suggests, passive attenuation methods use passive components, viz., inductors, capacitors, and resistors, which are simple to design, economical, and reliable [10]. The prevalent passive CM attenuation methods are the three-phase CM choke, the CM electromagnetic interference (EMI) filter, and the CMT with a damping resistor on the secondary side. Passive EMI filters with and without access to the neutral point of the machine are proposed in [11] and [12] to attenuate all CMV effects, such as shaft voltage, bearing current, and common-mode current (CMC). An integrated *LR* filter is proposed to reduce both the CM and differential-mode (DM) components [13]. To minimize both the peak amplitude and root-mean-square (rms) values of the CMC, a CMT with a secondary damping resistor is proposed [14] and is revisited for a high-power-rating machine with recurring bearing failure [15]. The modeling and design methods of a three-phase CM choke have been proposed to reduce the size of the CM choke for a given frequency range [16], [17]. The influence of CM volt–seconds on the choke saturation and the corresponding design guidelines are discussed in detail [18]. Although passive methods are well researched in terms of their applications, its size is yet to be optimized to increase the performance with advanced PWM techniques.

For a two-level inverter, the conventional topology is modified by adding a fourth leg to eliminate the CMV with reference to ground [19]. Many PWM methods such as active zero state PWM (AZPWM-1, AZPWM-2, and AZPWM-3), remote state PWM, and near state PWM have been proposed to mitigate

Manuscript received February 21, 2019; revised June 5, 2019; accepted July 17, 2019. Date of publication July 23, 2019; date of current version December 13, 2019. Recommended for publication by Associate Editor K.-B. Lee. *(Corresponding author: Kalaiselvi Jayaraman.)*

The authors are with the Department of Electrical Engineering, Indian Institute of Technology Ropar, Rupnagar 140001, India (e-mail: kalaiselvijeyaraman@gmail.com; 2016eez0010@iitrpr.ac.in).

Color versions of one or more of the figures in this paper are available online at http://ieeexplore.ieee.org.

Digital Object Identifier 10.1109/TPEL.2019.2930825

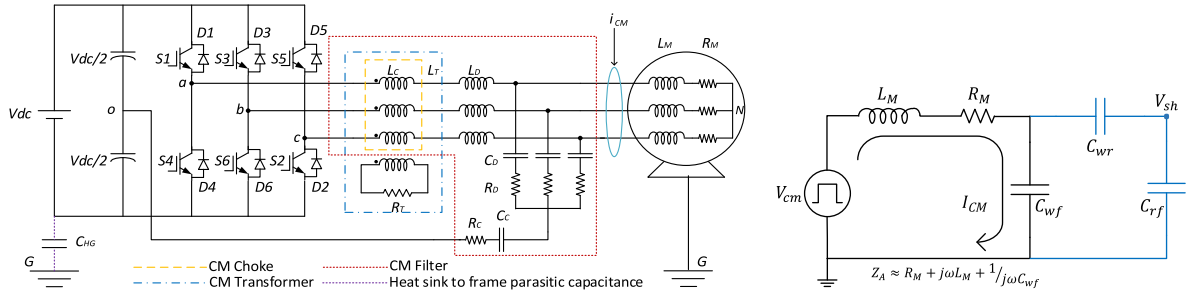

Fig. 1. (a) TLVSI power circuit with passive CM attenuation methods for the 3-ϕ IM drive. (b) Simplified CM equivalent circuit for the 3-ϕ IM drive.

the CMV in VFDs by avoiding zero vectors [20], [21]. AZPWM-1 has several advantages over other CMV reduction PWM techniques such as full control of linear modulation index and change in one switch state at a time [22]. However, performance of AZPWM-1 is inferior to that of space vector pulsewidth modulation (SVPWM) in terms of harmonic profile and voltage reversal issues. The voltage reversal problems can be modified by adjusting the zero vector time period and duty appropriately [20]. Therefore, AZPWM-1 can be applied to a high inductive motor [20]. The scalar implementation of AZPWM-1 and its compatibility issues with a pure sine wave filter are detailed in [22]. This PWM technique is successful in reducing the CM issues in the vicinity of switching frequency (F_s). However, the implementation does not guarantee the complete elimination of CM issues [22], [23]. Therefore, the usage of conventional passive methods (CM choke, CMT, and CM EMI filter) along with reduced CMV PWMs (such as AZPWM-1) to completely eliminate the end effects of CMV is inevitable. This calls for a need to redesign the passive methods with advanced CMV reduction PWM techniques such as AZPWM-1. The impact of AZPWM-1 on CMC, core saturation, and resonant frequency (F_{res}) is detailed in [23]. Here, F_s is varied freely with *RL* load and a fixed capacitance (imitating the parasitic behavior) to demonstrate the issues with advanced PWMs [23]. Such a study has to be conducted, in general, for VFDs, and the design guidelines for passive attenuation methods with AZPWM-1 have to be systematically formulated.

The objective of this paper is to verify the attenuation requirement of AZPWM-1 and propose the design guidelines for passive attenuation methods (CM choke, CMT with a damping resistor, and CM EMI filter) for a V/f-controlled induction motor (IM) drive. This paper further compares the passive component size and attenuation requirement for reducing CMC and shaft voltage with SVPWM. These attenuation methods can be extended to reduced CMV PWM methods with reduced peak amplitude and number of step changed levels of CMV [26], [27]. The effectiveness of envisaged passive methods for the inverter-fed IM drive is verified experimentally.

II. CMV, CMC, and Shaft Voltage for SVPWM and AZPWM-1 and Its Attenuation Requirements

The power topology of a two-level voltage-source inverter (TLVSI) with all the passive attenuation methods feeding a 3-ϕ IM drive is shown in Fig. 1(a).

TABLE I
CMV Contributions in the TLVSI

S. No	Switching states	CMV of TLVSI	S. No	Switching states	CMV of TLVSI
1.	1(100)	$-V_{dc}/6$	5.	5(001)	$-V_{dc}/6$
2.	2(110)	$+V_{dc}/6$	6.	6(101)	$+V_{dc}/6$
3.	3(010)	$-V_{dc}/6$	7.	7(111)	$+V_{dc}/2$
4.	4(011)	$+V_{dc}/6$	8.	8(000)	$-V_{dc}/2$

The CMV (v_{No} or v_{CM}) of the TLVSI is given as

$$v_{No} = v_{\text{CM}} = \frac{v_{ao} + v_{bo} + v_{co}}{3} \tag{1}$$

where v_{ao}, v_{bo}, and v_{co} represent the pole voltages. Each pole voltage of the TLVSI can attain two switching states at any instant, and as a result, eight switching states are possible for three legs. The CMVs for all eight switching states are listed in Table I. It establishes that the CMV attains its maximum value for seven and eight vectors. Based on this, AZPWM-1 is proposed to minimize various CMV-related issues by avoiding seven and eight vectors. It has been reported that the CMV of AZPWM-1 is reduced from $V_{\text{dc}}/2$ to $V_{\text{dc}}/6$ [20]–[22].

The magnitude difference between SVPWM and AZPWM-1 is derived to obtain worst-case operating conditions such as modulation index (m_a) and switching frequency (F_s). The magnitude of CMV for SVPWM [18] is given as

$$|v_{\text{CM}}|_{\text{SVPWM}} = T_0 \frac{|V_{\text{dc}}|}{2} + (T_s - T_0)\frac{|V_{\text{dc}}|}{6} \tag{2}$$

where T_0 is the period for realizing states 7 and 8, and T_S is the total switching period. The CMV of AZPWM-1 and SVPWM differs only during T_0 [22]. Therefore, the magnitude of CMV for AZPWM-1 is obtained by replacing $V_{\text{dc}}/2$ during T_0 [20], [22] with $V_{\text{dc}}/6$. As a result, we have

$$|v_{\text{CM}}|_{\text{AZPWM-1}} = T_0 \frac{|V_{\text{dc}}|}{6} + (T_s - T_0)\frac{|V_{\text{dc}}|}{6}. \tag{3}$$

The ratio of CMV magnitude between SVPWM and AZPWM-1 is given as

$$\frac{|v_{\text{CM}}|_{\text{SVPWM}}}{|v_{\text{CM}}|_{\text{AZPWM-1}}} = 1 + \frac{2T_0}{T_s}. \tag{4}$$

The difference in CMV magnitude between SVPWM and AZPWM-1 from (4) helps in deciding the attenuation difference between them. The difference in CMV magnitude is less when T_0/T_S is less. This leads to minimum magnitude difference

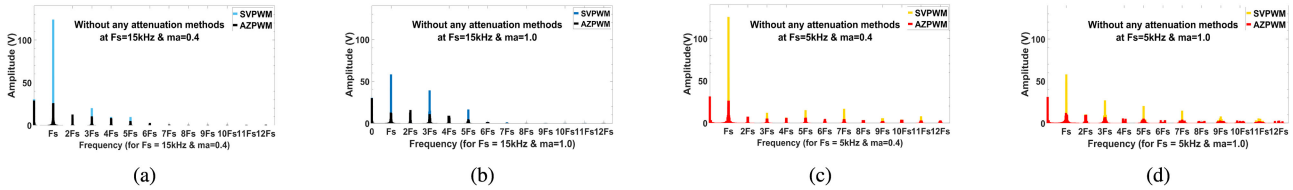

Fig. 2. FFT of CMV for SVPWM/AZPWM-1 (a) at 15 kHz ($m_a = 0.4$), (b) at 15 kHz ($m_a = 1.0$), (c) at 5 kHz ($m_a = 0.4$), and (d) at 5 kHz ($m_a = 1.0$) obtained experimentally without any attenuation methods.

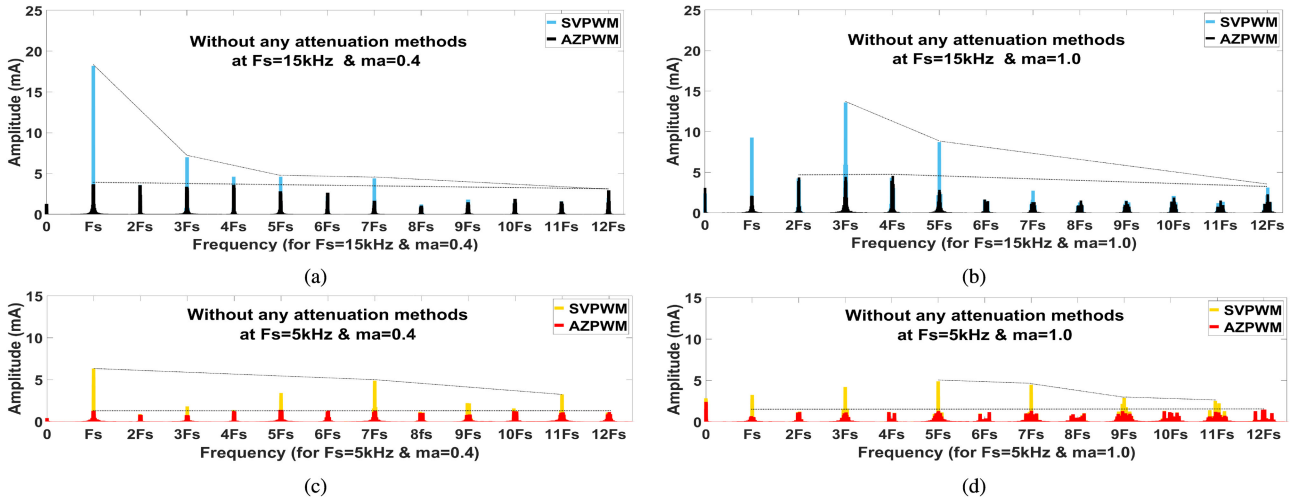

Fig. 3. FFT of CMC SVPWM/AZPWM-1 (a) at 15 kHz ($m_a = 0.4$), (b) at 15 kHz ($m_a = 1.0$), (c) at 5 kHz ($m_a = 0.4$), and (d) at 5 kHz ($m_a = 1.0$) obtained experimentally without any attenuation methods.

in the considered two PWMs. At high m_a, T_0/T_S is less due to the maximum voltage requirement at the motor terminals. Therefore, high m_a is the worst-case scenario for magnitude difference between CMV of SVPWM and AZPWM-1.

The CM equivalent of a 3-ϕ IM drive with CMV (v_{CM}) being the source for shaft voltage and CMC (i_{CM}) with parasitic capacitances is shown in Fig. 1(b), where C_{wf}, C_{wr}, and C_{rf} represent the capacitance between winding to frame, winding to rotor, and rotor to frame, respectively. Also, L_M and R_M represent the CM leakage inductance and resistance of the machine, respectively. C_{wf} is the most predominant parasitic component and contributes to most of the CMC [24]. The high-frequency v_{CM} excites the parasitic capacitances of the machine and generates high-frequency CMC, which mainly flows through C_{wf} and returns to the source based on the grounding scheme.

The expression of CMC is given as

$$I_{\text{CM}} = V_{\text{CM}}/Z_A. \tag{5}$$

The equivalent circuit [see Fig. 1(b)] is simplified as a capacitance divider, and the shaft voltage (V_{sh}) is given by (6). This also substantiates the concept that V_{sh} is a replica of CMV

$$v_{\text{sh}} = V_{\text{CM}} * \frac{C_{\text{wr}}}{C_{\text{wr}} + C_{\text{rf}}}. \tag{6}$$

The frequency-domain CMV profiles [V_{NG} of Fig. 1(a)] for SVPWM and AZPWM-1 at different operating conditions ($m_a = 0.4$ and 1.0 at $F_s = 5$–15 kHz) of the V/f-controlled IM drive are shown in Fig. 2(a)–(d). It is clear from the profiles that the odd multiples of F_s are greatly reduced for AZPWM-1 at all tested operating conditions. The magnitude of CMV for SVPWM and AZPWM-1 differs in time and frequency domains; hence, the attenuation requirements will be different. The size of passive attenuation methods mainly depends on the magnitude of F_s multiples of CMC; hence, several multiples of F_s are considered in this paper. The magnitude of CMC in the frequency domain for SVPWM and AZPWM-1 is plotted against each other for various operating conditions, as shown in Fig. 3(a)–(d). Here, the CMC is measured by clamping the three-phase wires using a current probe, as indicated in Fig. 1(a), and its frequency spectrum is obtained using a digital storage oscilloscope. The CM impedance of the machine is identical for both PWMs, so the CMC will also have the same inference as the CMV. However, the frequency at which the maximum CMC (see Fig. 3) occurs is inconsistent to that of CMV in Fig. 2. This is due to huge difference in the magnitude of CMV at F_s, $3F_s$, and $5F_s$ at low and high m_a and nonlinear impedance of the machine [23]. It is evident from Fig. 3 that the attenuation required for AZPWM-1 at several multiples of F_s is much lesser than SVPWM due to the magnitude difference of F_S components at all the measured operating conditions. Though at different switching frequencies, the magnitude of F_S multiples of the CMV remains almost the same (see Fig. 2), CMC components are increased due to

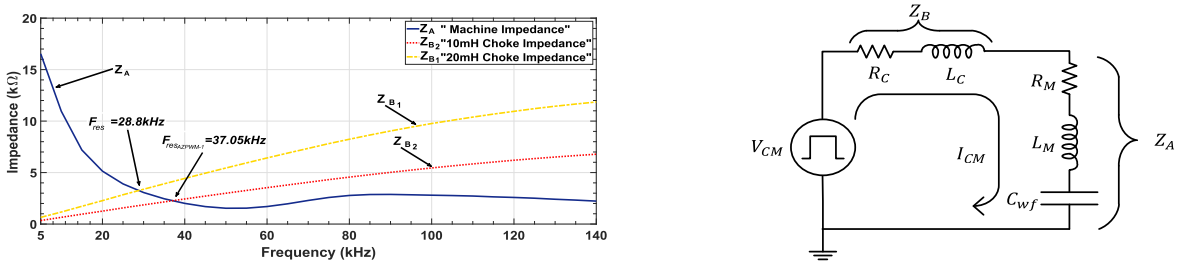

(a) (b)

Fig. 4. (a) CM impedance of the machine and choke measured by an *LCR* meter (linear scale). (b) CM equivalent circuit of the IM with a CM choke.

low impedance offered by the machine at those frequencies [see Fig. 4(a)]. Therefore, the worst-case attenuation difference between SVPWM and AZPWM-1 discussed in Section II is noted for high m_a and F_S, as evident from Fig. 3(b). This worst-case attenuation difference is defined as "n," which can also be estimated from the frequency inputs of the predicted/simulated CMV [29] and the CM impedance of the machine [14], [22], [28] as per (5). In this paper, a 1.1-kW IM is tested, and the worst-case attenuation difference at all operating conditions is obtained as $2.13 \approx 2$ (depending upon the nearest available choke value). The passive methods for both PWMs are designed for this worst-case operating condition.

III. Passive CM Attenuation Methods for the TLVSI-Fed IM Drive

In this section, the design guidelines of various passive CM attenuation methods for TLVSI [see Fig. 1(a)], which include CM choke, CM EMI filter, and CMT, are discussed.

A. CM Choke Design

The CM choke offers high impedance for the CMC of the drive system. However, due to low parasitic capacitive (C_{wf}) impedance of the machine (low output impedance of the choke), almost entire CMV appears across it. This would result in the existence of shaft voltage and bearing currents in the machine [17], [18], [23].

The simplified CM lumped equivalent circuit of IM without any attenuation method and with CM choke is shown in Figs. 1(b) and 4(b), respectively. The resonant frequency of the CM equivalent circuit with the CM choke is defined as

$$F_{\text{res}} = \frac{1}{2\pi\sqrt{L_C.C_{\text{wf}}}}. \tag{7}$$

The inductance of the CM choke (L_C) is decided based on the attenuation requirement and on the range of F_s components to be attenuated.

It can be observed from Fig. 3(a)–(d) that the dominant CMC components lie between F_s and $12F_s$. To eliminate a minimum of half the CMC components between F_s and $12F_s$, F_{res} is fixed between $3F_s$ and $5F_s$ for both the PWMs. Keeping $F_{\text{res}} \ll F_s$ will attenuate all the CMC components but demands a higher value of L_C, whereas $F_{\text{res}} \gg F_s$ leads to nonelimination of PWM frequency components. This is the first design choice to be made while choosing F_{res}. For the same F_{res}, a machine with a lower value of C_{wf} will require a larger value of L_C and vice versa as per (7). The range of C_{wf} for different motor ratings is given in [25]

$$I_{\text{CM(without choke)}} = V_{\text{CM}}/(Z_A) \tag{8}$$

$$I_{\text{CM(with choke)}} = V_{\text{CM}}/(Z_A + Z_B) \tag{9}$$

where $Z_A = R_M + j\omega L_M + 1/j\omega C_{wf}$ is the CM impedance of the machine, where $C_{\text{wf}} \approx 1.7$ nF (measured for 1.1-kW IM with an *LCR* meter [14], [25]) and $Z_B = R_C + j\omega L_C \approx j\omega L_C$ is the impedance of the CM choke. Z_{B_1} and Z_{B_2} are the CM impedances of the choke for SVPWM and AZPWM-1, respectively. For the worst-case scenario discussed in Section II, the impedance requirements for both the PWMs are related as

$$Z_{B_2} = Z_{B_1}/n. \tag{10}$$

Here, $n = 2$ for a 1.1-kW IM, as discussed in Section II. If the inductive impedance is reduced by a factor of 2, then the resonance frequency for AZPWM-1 can be found by substituting $L_C/2$ into (7). Therefore, the new resonance frequency for AZPWM-1 is chosen as

$$F_{\text{res}_{\text{AZPWM-1}}} = F_{\text{res}}/1.414. \tag{11}$$

Based on the above discussion, F_{res} is fixed at 28 kHz for SVPWM and 38 kHz for AZPWM-1 to eliminate the CM components above $3F_s$, for $F_s = 15$ kHz. As established from (7), (10), and (11), the required filter inductances for SVPWM and AZPWM-1 are about 20 and 10 mH, respectively. The CM impedance characteristics of the machine along with the three-phase CM choke for two different inductances measured by the *LCR* meter are shown in Fig. 4(a). It is also evident from Fig. 4(a) that the impedance doubles for every 1.41 times the reduction of resonance frequency. The CM choke among the passive methods is the least effective in attenuating the shaft voltage [22].

B. CM EMI Filter Design

The passive EMI filter consists of a CM filter (L_C, C_C, and R_C) and a DM filter (L_D, C_D, and R_D) to reduce both CM and DM components, as shown in Fig. 1(a) [12]. The use of the CM filter alone is not suitable for the TLVSI due to huge circulating currents between the CM capacitors and resistors [12], [31]. To keep the DM attenuation constant,

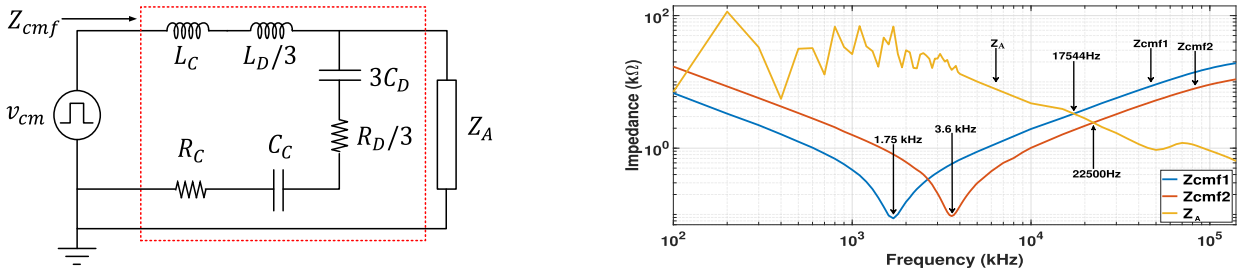

Fig. 5. (a) CM equivalent circuit of the IM with a CM EMI filter. (b) CM impedance of the IM and CM EMI filter measured by the *LCR* meter (logarithmic scale).

a DM filter is added uniformly for both the PWMs. However, in this paper, both CM and DM filters are considered while designing the CM EMI filter, as shown in Fig. 5(a). The design of L_{CM}, C_{CM}, and R_{CM} is given as

$$L_{\text{CM}} = L_C + L_D/3 \tag{12}$$

$$C_{\text{CM}} = (C_C \times C_D)/(C_C + C_D) \quad \& \quad R_{\text{CM}} = R_C + R_D/3 \tag{13}$$

$$\delta = \frac{R_{\text{CM}}}{2}\sqrt{\frac{L_{\text{CM}}}{C_{\text{CM}}}}. \tag{14}$$

The CM filter consists of L_{CM}, C_{CM}, and R_{CM} such that most of the CMCs are attenuated by L_{CM} ($j\omega L_{\text{CM}} >> 1/j\omega C_{\text{CM}}$), and rest of them are bypassed by the filter capacitor (C_{CM}) by choosing $C_{\text{CM}} \gg C_{\text{wf}}$. Thus, it can provide the complete solution for the reduction of conduction-mode EMI, shaft voltage, and bearing current [12], [22].

The required damping for the second-order CM filter is provided by R_{CM}. A DM filter with a resonant frequency of 2.5 kHz is fixed uniformly for both the PWMs. The CM filter design for SVPWM is given in [12]. The resonant frequency of the CM filter is placed much higher than $3f$ (where f is the fundamental output frequency) and much less than F_s, i.e., ($3f \ll F_{\text{res}_{\text{cmf}}} \ll F_s$). Therefore, $F_{\text{res}_{\text{cmf}}}$ of the CM filter is given as

$$F_{\text{res}_{\text{cmf}}} = \frac{1}{2\pi\sqrt{L_{\text{CM}}.C_{\text{CM}}}}. \tag{15}$$

In the worst-case scenario, the impedance requirement of AZPWM-1 is half that of SVPWM. The CM inductance (L_C) and capacitance (C_C) for the worst-case attenuation are given as

$$L_{C_{\text{AZPWM-1}}} = L_{C_{\text{SVPWM}}}/n \tag{16}$$

$$C_{C_{\text{AZPWM-1}}} = C_{C_{\text{SVPWM}}}/n. \tag{17}$$

The resonance frequency of the CM filter in the case of AZPWM-1 can be chosen at least two times that of SVPWM. Following are some of the guidelines for the CM EMI filter.

1) If F_s is less, then keeping $F_{\text{res}_{\text{cmf}}} \ll F_s$ results in an increased size of the passive components.
2) Design of the CM filter requires $C_C \gg C_{\text{wf}}$ to offer low impedance to CMC. This is easier to achieve in machines with a lower value of C_{wf}.

The F_{res} of the CM filter is fixed based on the above discussion as 1.75 kHz for SVPWM and 3.6 kHz for AZPWM-1. The damping factor (δ) is chosen as 0.08 for both the PWMs. In the worst-case scenario, the impedance requirement of AZPWM-1 is reduced by two times to that of SVPWM.

In summary, the designed CM EMI filter components for SVPWM and AZPWM-1 based on (12)–(17) are as follows:

$$L_C = 27.3\,\text{mH}, C_C = 0.3\,\mu\text{F}, R_C = 50\,\Omega \text{ for SVPWM} \tag{18}$$

$$L_C = 15.2\,\text{mH}, C_C = 0.15\,\mu\text{F}, R_C = 50\,\Omega \text{ for AZPWM-1}. \tag{19}$$

To complete the design details of the EMI filter, the DM filter components are given as follows [12]:

$$L_D = 8\,\text{mH},\ C_D = 0.5\,\mu\text{F},\ R_D = 14\,\Omega,\ \text{and}\ F_{\text{DM}} = 2.5\,\text{kHz}. \tag{20}$$

The impedance characteristics of the designed filters for SVPWM and AZPWM-1 are shown in Fig. 5(b). Here, Z_{cmf1} and Z_{cmf2} are the equivalent CM impedances for SVPWM and AZPWM-1, respectively. It is evident from Fig. 5(b) that to have the same attenuation for both SVPWM and AZPWM-1, the $F_{\text{res}_{\text{cmf}}}$ of AZPWM-1 is designed to be higher than that of the SVPWM.

C. CMT Design

Similar to the CM choke, the CMT consists of an additional fourth winding connected to a damping resistor R_T [as shown in Fig. 1(a)] to damp out CMC oscillations. The magnetizing inductance L_T and R_T are designed to limit the rms and peak values of the CMC. The CM equivalent of the CMT is shown in [14]. It can be simplified as a series *RC* circuit when the roots of denominator polynomial with the obtained transfer function are tuned appropriately. The rms value of CMC (I_{rms}) can be estimated from the equivalent *RC* circuit if C_{wf} of the machine is known [14]

$$I_{\text{rms}} = E\sqrt{\frac{3C_{\text{wf}}.F_S}{R_T}} \tag{21}$$

$$R_T = \frac{3C_{\text{wf}}E^2.F_S}{I_{\text{rms}}^2}. \tag{22}$$

Here, E is the stepwise change in the CMV, i.e., $V_{\text{dc}}/3$ [14], where V_{dc} is the dc-bus voltage of the inverter. The desired value

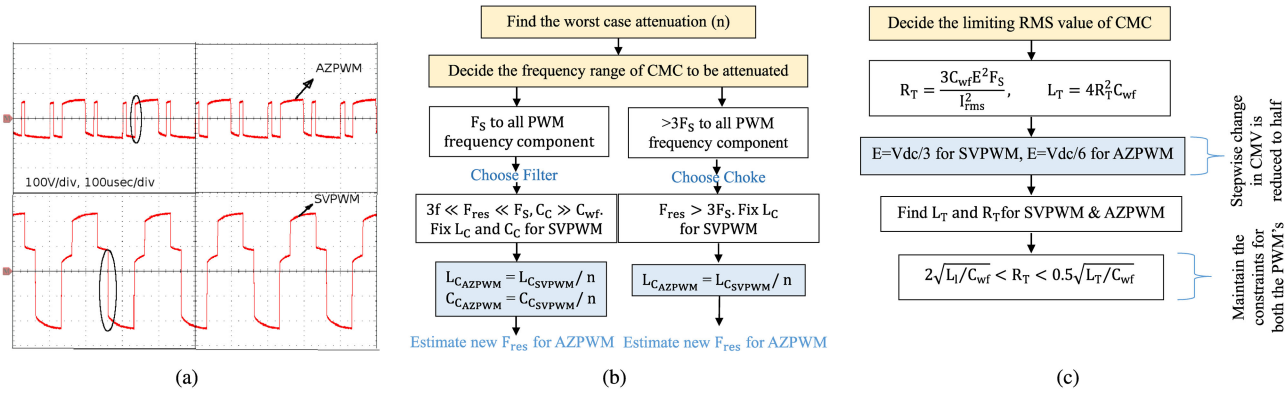

(a) (b) (c)

Fig. 6. (a) CMV of the inverter with SVPWM and AZPWM-1 showing worst-case step change. (b) Flowchart for the design of choke and filter for SVPWM and AZPWM-1. (c) Flowchart for the design of the CMT with a damping resistor.

of L_T can be obtained as

$$L_T = 4R_T^2 \times C_{\text{wf}}. \tag{23}$$

The higher value of F_s and E increases the value of L_T. To minimize the rms values of the CMC, the design should meet the following constraint:

$$2\sqrt{\frac{L_l}{C_{\text{wf}}}} < R_T < \frac{1}{2}\sqrt{\frac{L_T}{C_{\text{wf}}}}. \tag{24}$$

Here, L_l is the sum of the leakage inductance of the machine and the cable. Some of the design choices for limiting L_T are lower F_S and machine with a lower value of C_{wf}. In the worst case, the rate of change in CMV for AZPWM-1 is half that of SVPWM, as depicted in Fig. 6(a). It occurs when time intervals are smaller than the CMV transients. Therefore, E for AZPWM-1 is half that of SVPWM, i.e., $V_{\text{dc}}/6$. To limit the rms value of CMC to 13.0 mA for both the PWMs at F_s of 5 kHz, the values of R_T and L_T are found using (22) and (23) and are shown as follows:

$$\text{SVPWM} : L_T = 27.89\,\text{mH}, R_T = 2.05\,\text{k}\Omega \tag{25}$$

$$\text{AZPWM-1} : L_T = 10.41\,\text{mH}, R_T = 1.3\,\text{k}\Omega. \tag{26}$$

Comparing the design of CMT in both the cases, it can be observed that L_T for AZPWM-1 is almost one-third of its value from SVPWM. An alternate design option is to increase the F_s of AZPWM-1 with the same L_T as in SVPWM.

The design procedure for all three methods is shown in Fig. 6(b) and (c). For designing the CM choke and the EMI filter, it is necessary to determine the worst-case magnitude attenuation difference between SVPWM and AZPWM-1 (n). The CM EMI filter is chosen to attenuate all the PWM frequency components from F_s. If the attenuation requirement is from $3F_s$ or $5F_s$, then the CM choke is a better choice, as the burden on hardware is less. Compared to abovementioned methods, the design of the CMT does not require any prediction/hardware procedure except finding C_{wf}.

IV. Results and Discussion

The experimental setup consists of 1.1-kW IM, 4-kVA inverter, and DSP-F28377S controller, as shown in Fig. 7(a). The IM parameters and TLVSI operating conditions are presented in Fig. 7(b), and the IM is modified to measure the shaft voltage, as in [26]. The maximum linear m_a for SVPWM and AZPWM-1 is 1.15 [22], [30]. To limit the size of passive components, F_s for the CM choke and the EMI filter is fixed at 15 kHz, and for CMT, it is fixed at 5 kHz. The experimentally obtained phase voltages and currents of the TLVSI without and with passive attenuation methods for both SVPWM and AZPWM-1 are shown in Fig. 8. It can be seen in Fig. 8(a)–(f) that the phase profiles remain the same without and with the CM choke and the CMT. However in Fig. 8(g) and (h), due to an additional DM filter in the CM EMI filter, both the phase voltage and the current are sinusoidal.

The design of the CM choke and the EMI filter is based on frequency-domain profiles, and hence, experimentally obtained fast Fourier transforms (FFTs) of the CMC without and with passive attenuation methods are shown in Figs. 3 and 9. It can be seen from Figs. 3(a), (b) and 9(a), (b) that the CM choke for both the PWMs eliminates the F_s multiples above F_{res} ($>3F_s$). With the CM EMI filter in Fig. 9(c) and (d), all F_s multiples are attenuated.

The experimentally obtained time-domain profiles of the CMC without and with the CM choke and the CM EMI filter for both the PWMs are shown in Fig. 10. This shows that with reduced hardware components, AZPWM-1 attenuates the peak amplitude and the rms value of CMC similar to SVPWM. Similarly, the experimentally obtained CMV and shaft voltage of CMV without and with the CM choke and the CM EMI filter for both the PWMs are shown in Fig. 11. The peak magnitude and dv/dt of CMV and shaft voltages sees very less attenuation with the CM choke, as shown in Fig. 11(b) and (e), whereas with the CM EMI filter, both the peak magnitude and dv/dt of CMV and shaft voltage attenuation is maximum, as shown in Fig. 11(c) and (f).

The experimental results without and with CMT at F_s of 5 kHz are shown in Figs. 12 and 13, respectively. It is clear from Fig. 13(a) and (b) that the desired rms value of the CMC at

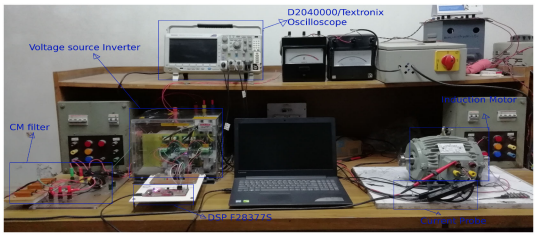

(a)

Sr.No.	Item	Parameters
1.	IM	$1.1kW, 415V, 50Hz, 2.55A, Stator\ Resistance, R_s = Rotor\ Resistance, R'_r = 6.53\Omega, Stator\ Inductance, L_s = Rotor\ Inductance; L'_r = 39.559mH, Core\ Loss\ Component, R_c = 1266.3\Omega, ; Magnetizing\ Inductance, L_m = 0.542H$
2.	Operating	$V_{dc} = 450Volt, F_S = 5kHz\ \&15kHz, m_a = 0.4\ \&\ 1$
3.	CM Choke	$L_{C_{AZPWM}} = 20mH, L_{C_{SVPWM}} = 10mH$
4.	CM Filter	$SVPWM: L_C = 27.3mH, C_C = 0.3uF, R_C = 50\Omega;$ $AZPWM: L_C = 15.2mH, C_C = 0.15uF, R_C = 50\Omega$
5.	CMT	$SVPWM: L_T = 27.89mH, R_T = 2.05k\Omega;$ $AZPWM: L_T = 15.2mH, R_T = 1.3k\Omega$

(b)

Fig. 7. (a) Experimental setup consisting of an inverter with a CM filter feeding an IM. (b) Experimental and IM parameters, operating conditions, and design specifications.

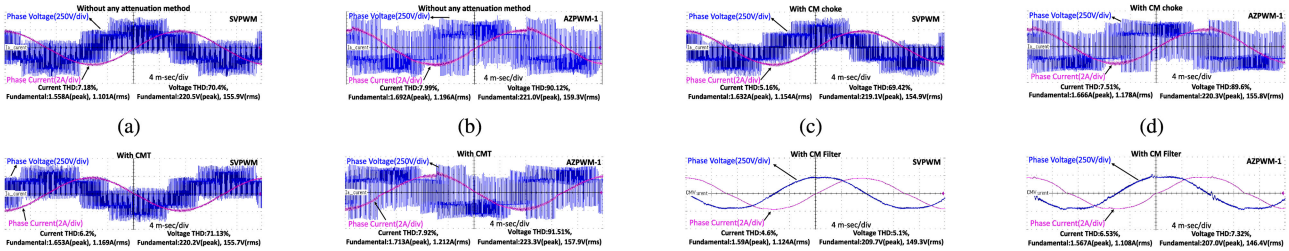

(a) (b) (c) (d) (e) (f) (g) (h)

Fig. 8. Experimentally obtained IM phase voltage and no-load current waveforms, without any attenuation methods for (a) SVPWM at 5 kHz and (b) AZPWM-1 at 5 kHz, with the CM choke for (c) SVPWM at 5 kHz and (d) AZPWM-1 at 5 kHz, with the CMT for (e) SVPWM at 5 kHz and (f) AZPWM-1 at 5 kHz, and with the CM EMI filter for (g) SVPWM at 15 kHz and (h) AZPWM-1 at 15 kHz.

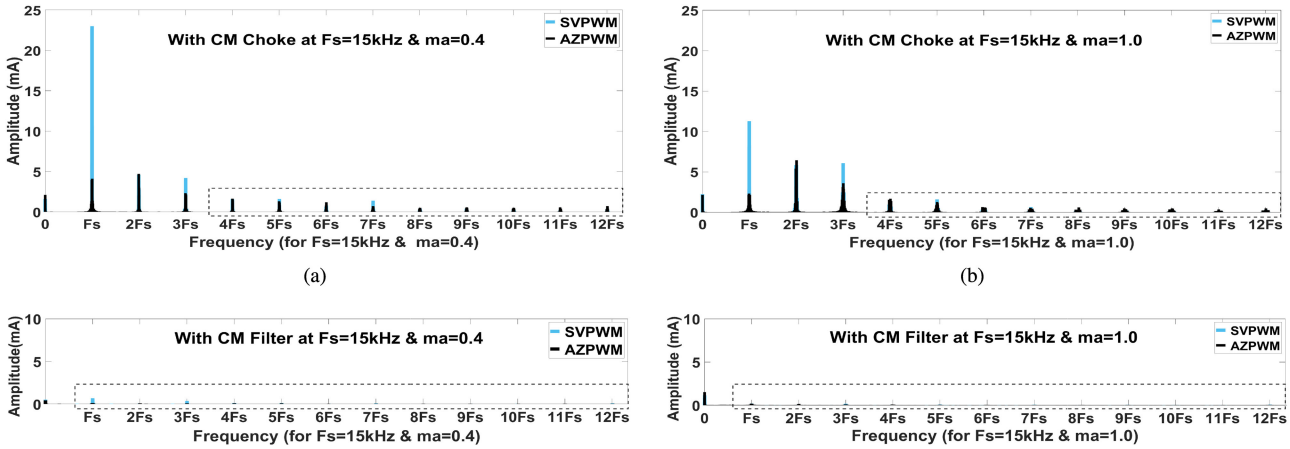

(a) (b) (c) (d)

Fig. 9. Experimental obtained FFT of CMC for SVPWM and AZPWM-1 with the CM choke at (a) $F_s = 15$ kHz and $m_a = 0.4$ and (b) $F_s = 15$ kHz and $m_a = 1.0$ and with the CM EMI filter at (c) $F_s = 15$ kHz and $m_a = 0.4$ and (d) $F_s = 15$ kHz and m_a=1.0.

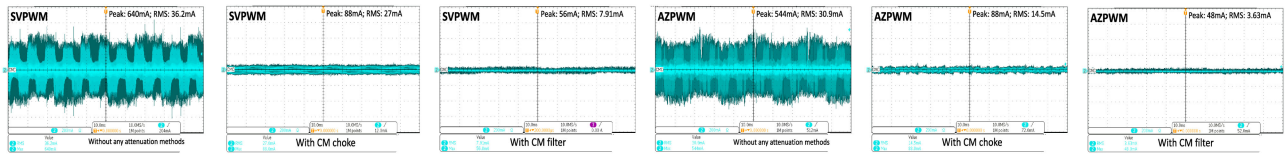

(a) (b) (c) (d) (e) (f)

Fig. 10. Experimentally obtained time-domain profile of the CMC for SVPWM at $F_s = 15$ kHz (a) without attenuation, (b) with the CM choke, (c) with the CM EMI filter, and for AZPWM-1 at $F_s = 15$ kHz (d) without attenuation, (e) with the CM choke, and (f) with the CM EMI filter.

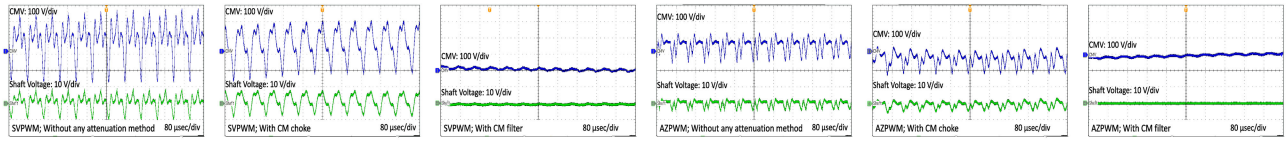

(a) (b) (c) (d) (e) (f)

Fig. 11. Experimentally obtained time domain profile of CMV and shaft voltage for SVPWM at $F_s = 15$ kHz (a) without attenuation, (b) with the CM choke, and (c) with the CM EMI filter, and for AZPWM-1 at $F_s = 15$ kHz (d) without attenuation, (e) with the CM choke, and (f) with the CM EMI filter.

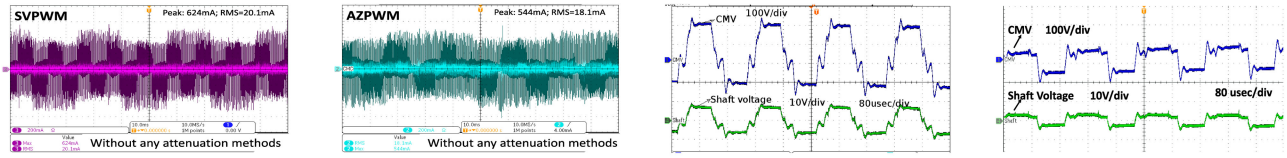

(a) (b) (c) (d)

Fig. 12. Experimentally obtained time-domain profile of CMC for (a) SVPWM and (b) AZPWM-1, and CMV and shaft voltage for (c) SVPWM and (d) AZPWM-1 without the attenuation method at $F_s = 5$ kHz and $m_a = 0.4$.

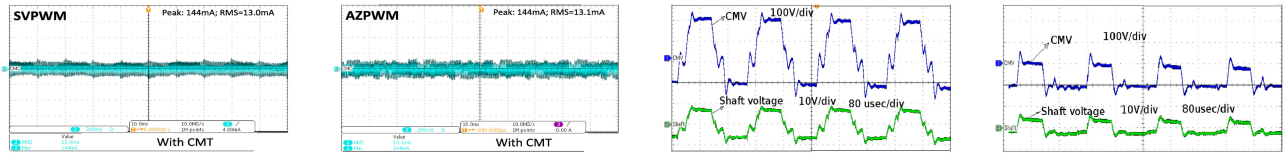

(a) (b) (c) (d)

Fig. 13. Experimentally obtained time domain profile of CMC for (a) SVPWM and (b) AZPWM-1, and CMV and shaft voltage for (c) SVPWM and (d) AZPWM-1 with the CMT at $F_s = 5$ kHz and $m_a = 0.4$.

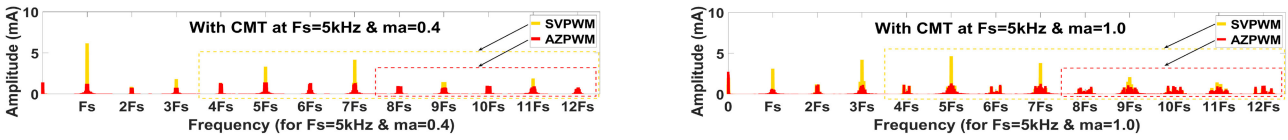

(a) (b)

Fig. 14. Experimentally obtained FFT of CMC for SVPWM and AZPWM-1 with CMT at $F_s = 5$ kHz and (a) $m_a = 0.4$ and (b) $m_a = 1.0$.

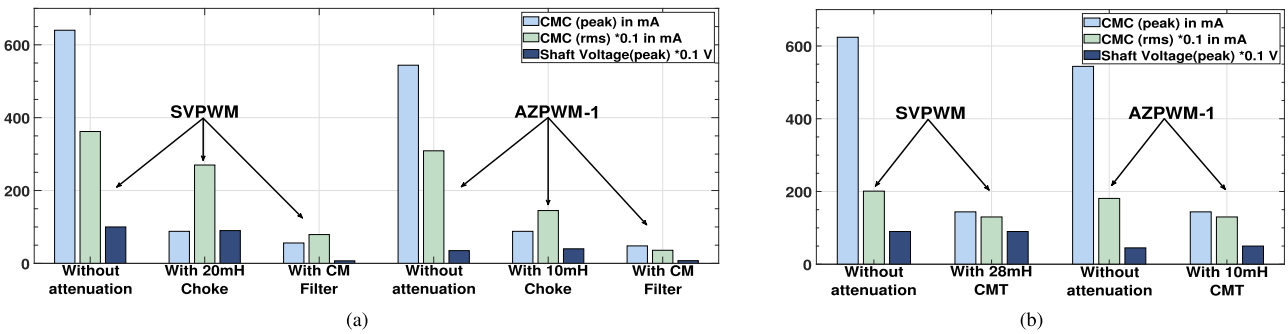

(a) (b)

Fig. 15. Experimental results for comparison of peak and rms values of CMC and peak amplitude of shaft voltage without and with passive attenuation methods for (a) SVPWM and AZPWM-1 at $F_s = 15$ kHz and $m_a = 1.0$ and (b) SVPWM and AZPWM-1 at $F_s = 5$ kHz and $m_a = 0.4$.

$m_a = 0.4$ is 13 mA. With 2.68 times reduced L_T value, AZPWM-1 with the CMT provides the same rms value as designed. The peak values are comparable in all the cases. The CMV and shaft voltage profiles are shown in Fig. 13(c) and (d). The peak amplitude and dv/dt of the CMV and shaft voltage sees very little attenuation, as shown in Fig. 13. The FFT of the CMC without and with the CMT is shown in Figs. 3(c), (d) and 14(a), (b), where the F_s multiples above $F_{\text{res}}(>3F_S)$ for SVPWM and $F_{\text{res}}(>7F_S)$ for AZPWM are being attenuated.

Finally, the time-domain results without and with passive CM attenuation methods are compared for both the PWMs at $m_a = 0.4$ and 1 and $F_S = 5$ 15 kHz. The peak and rms values of CMC and peak amplitude of shaft voltage for different passive attenuation methods are shown in Fig. 15. Compared to SVPWM, it is seen that AZPWM-1 with two times lesser value of L_C and C_C results in similar attenuation of CMC and shaft voltage, whereas the CMT with 2.68 times lesser L_T has similar attenuation to CMC and shaft voltage. Therefore AZPWM-1 with lesser hardware can achieve equivalent CM performance for the TLVSI-fed IM drive.

V. Conclusion

This paper presented the design of passive CM attenuation methods for AZPWM-1 and compared their performance with that of conventional SVPWM. These design guidelines were realized based on the worst-case attenuation of CMC requirements for SVPWM and AZPWM-1. The component size in the case of AZPWM-1 was halved in comparison with that of SVPWM for the same attenuation of the tested IM drive. The reduction in CM inductances and capacitances resulted in reduced space, size, and cost. The contributions of this paper were to bring out the attenuation requirements for SVPWM and AZPWM-1 and the design guidelines of each passive method for AZPWM-1. Also, the limitations in terms of the increase in the size of passive components were presented.

References

[1] N. Das and M. K. Kazimierczuk, "Applications of silicon carbide power devices in three-phase voltage-fed induction motor drives for electric vehicles," in *Proc. Elect. Insul. Conf. Elect. Manuf. Expo*, Nashville, TN, USA, 2007, pp. 278–285.

[2] A. H. Bonnett, "Analysis of the impact of pulse-width modulated inverter voltage waveforms on AC induction motors," *IEEE Trans. Ind. Appl.*, vol. 32, no. 2, pp. 386–392, Mar./Apr. 1996.

[3] T. Plazenet, T. Boileau, C. Caironi, and B. Nahid-Mobarakeh, "A comprehensive study on shaft voltages and bearing currents in rotating machines," *IEEE Trans. Ind. Appl.*, vol. 54, no. 4, pp. 3749–3759, Jul./Aug. 2018.

[4] W. Chen, X. Yang, J. Xue, and F. Wang, "A novel filter topology with active motor CM impedance regulator in PWM ASD system," *IEEE Trans. Ind. Electron.*, vol. 61, no. 12, pp. 6938–6946, Dec. 2014.

[5] C. Mei, J. C. Balda, and W. P. Waite, "Cancellation of common-mode voltages for induction motor drives using active method," *IEEE Trans. Energy Convers.*, vol. 21, no. 2, pp. 380–386, Jun. 2006.

[6] S. Wang, Y. Y. Maillet, F. Wang, D. Boroyevich, and R. Burgos, "Investigation of hybrid EMI filters for common-mode EMI suppression in a motor drive system," *IEEE Trans. Power Electron.*, vol. 25, no. 4, pp. 1034–1045, Apr. 2010.

[7] D. Xu, C. K. Lee, S. Kiratipongvoot, and W. M. Ng, "An active EMI choke for both common- and differential-mode noise suppression," *IEEE Trans. Ind. Electron.*, vol. 65, no. 6, pp. 4640–4649, Jun. 2018.

[8] J. Huang and H. Shi, "A hybrid filter for the suppression of common-mode voltage and differential-mode harmonics in three-phase inverters with CPPM," *IEEE Trans. Ind. Electron.*, vol. 62, no. 7, pp. 3991–4000, Jul. 2015.

[9] S. Takahashi, S. Ogasawara, M. Takemoto, K. Orikawa, and M. Tamate, "Common-mode voltage attenuation of an active common-mode filter in a motor drive system fed by a PWM inverter," *IEEE Trans. Ind. Appl.*, vol. 55, no. 3, pp. 2721–2730, May/Jun. 2019.

[10] V. Dzhankhotov and J. Pyrhonen, "Passive LC filter design considerations for motor applications," *IEEE Trans. Ind. Electron.*, vol. 60, no. 10, pp. 4253–4259, Oct. 2013.

[11] H. Akagi and S. Tamura, "A passive EMI filter for eliminating both bearing current and ground leakage current from an inverter-driven motor," *IEEE Trans. Power Electron.*, vol. 21, no. 5, pp. 1459–1469, Sep. 2006.

[12] H. Akagi, H. Hasegawa, and T. Doumoto, "Design and performance of a passive EMI filter for use with a voltage-source PWM inverter having sinusoidal output voltage and zero common-mode voltage," *IEEE Trans. Power Electron.*, vol. 19, no. 4, pp. 1069–1076, Jul. 2004.

[13] R. M. Tallam, G. L. Skibinski, T. A. Shudarek, and R. A. Lukaszewski, "Integrated differential-mode and common-mode filter to mitigate the effects of long motor leads on AC drives," *IEEE Trans. Ind. Appl.*, vol. 47, no. 5, pp. 2075–2083, Sep./Oct. 2011.

[14] S. Ogasawara and H. Akagi, "Modeling and damping of high-frequency leakage currents in PWM inverter-fed AC motor drive systems," *IEEE Trans. Ind. Appl.*, vol. 32, no. 5, pp. 1105–1114, Sep./Oct. 1996.

[15] R. D. S. Arajo, R. D. A. Rodrigues, H. de Paula, B. J. C. Filho, L. M. R. Baccarini, and A. V. Rocha, "Premature wear and recurring bearing failures in an inverter-driven induction motor—Part II: The proposed solution," *IEEE Trans. Ind. Appl.*, vol. 51, no. 1, pp. 92–100, Jan./Feb. 2015.

[16] H. Chen and S. Ye, "Modeling of common-mode impedance of an inverter-fed induction motor from online measurement," *IEEE Trans. Electromagn. Compat.*, vol. 60, no. 5, pp. 1581–1589, Oct. 2018.

[17] M. L. Heldwein, L. Dalessandro, and J. W. Kolar, "The three-phase common-mode inductor: Modeling and design issues," *IEEE Trans. Ind. Electron.*, vol. 58, no. 8, pp. 3264–3274, Aug. 2011.

[18] F. Luo *et al.*, "Analysis of CM volt-second influence on CM inductor saturation and design for input EMI filters in three-phase DC-fed motor drive systems," *IEEE Trans. Power Electron.*, vol. 25, no. 7, pp. 1905–1914, Jul. 2010.

[19] A. L. Julian, G. Oriti, and T. A. Lipo, "Elimination of common-mode voltage in three-phase sinusoidal power converters," *IEEE Trans. Power Electron.*, vol. 14, no. 5, pp. 982–989, Sep. 1999.

[20] A. M. Hava and E. Un, "Performance analysis of reduced common mode voltage PWM methods and comparison with standard PWM methods for three-phase voltage-source inverters," *IEEE Trans. Power Electron.*, vol. 24, no. 1, pp. 241–252, Jan. 2009.

[21] A. M. Hava and E. Ün, "A high-performance PWM algorithm for common-mode voltage reduction in three-phase voltage source inverters," *IEEE Trans. Power Electron.*, vol. 26, no. 7, pp. 1998–2008, Jul. 2011.

[22] N. O. Cetin, "Design and implementation of advanced pulse width modulation techniques and passive filters for voltage source inverter driven three phase AC motors," Master's Thesis, Dept. Elect. Electron. Eng., Middle East Tech. Univ., Ankara, Turkey, Jul. 2010. [Online]. Available: http://etd.lib.metu.edu.tr/upload/12612236/index.pdf

[23] D. Jiang, F. Wang, and J. Xue, "PWM impact on CM noise and AC CM choke for variable-speed motor drives," *IEEE Trans. Ind. Appl.*, vol. 49, no. 2, pp. 963–972, Mar./Apr. 2013.

[24] J. M. Erdman, R. J. Kerkman, D. W. Schlelgel, and G. L. Skibinski, "Effect of PWM inverters on AC motor bearing currents and shaft voltages," *IEEE Trans. Ind. Appl.*, vol. 32, no. 2, pp. 250–259, Mar./Apr. 1996.

[25] A. Muetze, "Bearing currents in inverter fed AC motors," Ph.D. dissertation, Dept. Elect. Eng. Inf. Technol., Tech. Univ. Darmstadt, Darmstadt, Germany, 2004. [Online]. Available: https://www.ew.tu-darmstadt.de/media/ew/dissertationen/dissannette.pdf

[26] J. Kalaiselvi and S. Srinivas, "Bearing current profiles in a 3-phase VSI fed induction motor drive using a simplified measurement approach," in *Proc. IEEE Int. Conf. Power Electron., Drives Energy Syst.*, Dec. 16–19, 2012, pp. 1–6.

[27] J. Kalaiselvi and S. Srinivas, "Bearing currents and shaft voltage reduction in dual-inverter-fed open-end winding induction motor with reduced CMV PWM methods," *IEEE Trans. Ind. Electron.*, vol. 62, no. 1, pp. 144–152, Jan. 2015.

[28] N. Boucenna, F. Costa, S. Hlioui, and B. Revol, "Strategy for predictive modeling of the common-mode impedance of the stator coils in AC machines," *IEEE Trans. Ind. Electron.*, vol. 63, no. 12, pp. 7360–7371, Dec. 2016.

[29] Y. Han, H. Lu, Y. Li, and J. Chai, "Analysis and suppression of shaft voltage in SiC-based inverter for electric vehicle applications," *IEEE Trans. Power Electron.*, vol. 34, no. 7, pp. 6276–6285, Jul. 2019.
[30] H. W. van der Broeck, H.-C. Skudelny, and G. V. Stanke, "Analysis and realization of a pulsewidth modulator based on voltage space vectors," *IEEE Trans. Ind. Appl.*, vol. 24, no. 1, pp. 142–150, Jan./Feb. 1988.
[31] M. M. Swamy, J. Kang, and K. Shirabe, "Power loss, system efficiency, and leakage current comparison between Si IGBT VFD and SiC FET VFD with various filtering options," *IEEE Trans. Ind. Appl.*, vol. 51, no. 5, pp. 3858–3866, Sep./Oct. 2015.

Kalaiselvi Jayaraman received the B.E. degree in electrical and electronics engineering from Periyar University, Salem, India, in 2003, the M.E. degree in power electronics and drives from Anna University, Chennai, India, in 2005, and the Ph.D. degree from the Indian Institute of Technology Madras, Chennai, in 2015.

She is currently an Assistant Professor with the Department of Electrical Engineering, Indian Institute of Technology Ropar, Rupnagar, India. Her research interests include conduction-mode electromagnetic interference issues in Si and SiC inverter-fed drives and solid-state transformers for renewable energy integration to grids and microgrids.

Manish Kumar (S'18) received the B.Tech. degree in electrical and electronics engineering from Jawaharlal Nehru Technological University, Hyderabad, India, in 2013, and the M.E. degree in electrical engineering from the Birla Institute of Technology, Mesra, Ranchi, India, in 2016. He is currently working toward the Ph.D. degree in electrical engineering with the Indian Institute of Technology Ropar, Rupnagar, India.

His research interests include conducted electromagnetic interference (EMI) issues in pulsewidth-modulated inverters, design of EMI filters, and miniaturization of drive size.